Volcano-tectonics of the Al Haruj Volcanic Province, Central Libya

Abdelsalam Elshaafi[1], Agust Gudmundsson[1]

[1]Department of Earth Sciences, Royal Holloway University of London, Egham TW20 0EX, UK (abdelsalamelshaafi@yahoo.co.uk; a.gudmundsson@rhul.ac.uk)

Abstract

The Al Haruj intra-continental Volcanic Province (AHVP), located at the south-western margin of the Sirt Basin, hosts the most extensive and recent volcanic activity in Libya - which is considered typical for plate interiors. From north to south the AHVP is divided into two subprovinces, namely Al Haruj al Aswad and Al Haruj al Abiyad. The total area of the AHVP is around 42,000km^2. Despite the great size of the AHVP, its volcano-tectonic evolution and activity have received very little attention and are poorly documented and understood. Here we present new field data, and analytical and numerical results, on the volcano-tectonics of the AHVP. The length/thickness ratio of 47 dykes and volcanic fissures were measured to estimate magmatic overpressure at the time of eruption. The average dyke (length/thickness) ratio of 421 indicates magmatic overpressures during the associate fissure eruptions of 8 - 19MPa (depending on host-rock elastic properties). Spatial distributions of 432 monogenetic eruptions sites/points (lava shields, pyroclastic cones) in the AHVP reveal two main clusters, one in the south and another in the north. Aligned eruptive vents show the dominating strike of volcanic fissures/feeder-dykes as WNW-ESE to NW-SE, coinciding with the orientation of one of main fracture/fault zones. Numerical modelling and field

observations suggest that some feeder-dykes may have used steeply dipping normal-fault zones as part of their paths to the surface.

Keywords: Lava shields, Pyroclastic cones, Volcanic fissures, Feeder-dykes, Local stresses, Magma paths

1 Introduction

The Al Haruj Volcanic Province (AHVP) is the largest volcanic province in Libya, the other three being the Gharyan Province in north-western Tripoli, the Jabal as Sawda Volcanic Province, located between Jabal Gharyan Volcanic Province and the AHVP, and the Jabal Nuqay Volcanic Province which is situated close to Tibesti Mountain at the Libyan-Chadian border (Fig. 1a; Al-Hafdth and El-Shaafi., 2015). All four are considered typical intra-plate volcanic provinces. The AHVP developed from early Pliocene up to late Pleistocene and has been linked to the tectonic evolution of the rifting of the Sirt Basin (Less et al., 2006; Cvetkovic et al., 2010; Bardintzeff et al., 2012).

The AHVP is primarily composed of lava flows, mostly transitional to alkaline basalts and subsidiary sub-alkaline. More evolved volcanic rocks have not been observed (Busrewil and Suwesi, 1993; Peregi et al., 2003; Al-Hafdth and El-Shaafi., 2015). The area of the AHVP calculated using ArcGIS 10.1 during this study is around 42,000 km^2. The AHVP is here divided into two subprovinces based on volcano-morphological features and thicknesses of lava flows (Fig. 1b; Peregi et al., 2003). The main subprovince, which also shows the most recent volcanic activity, is the one located in the north. It is named the Al Haruj al Aswad Subprovince (AHAS) (the Black Mountain) and is mainly composed of lava flows younger

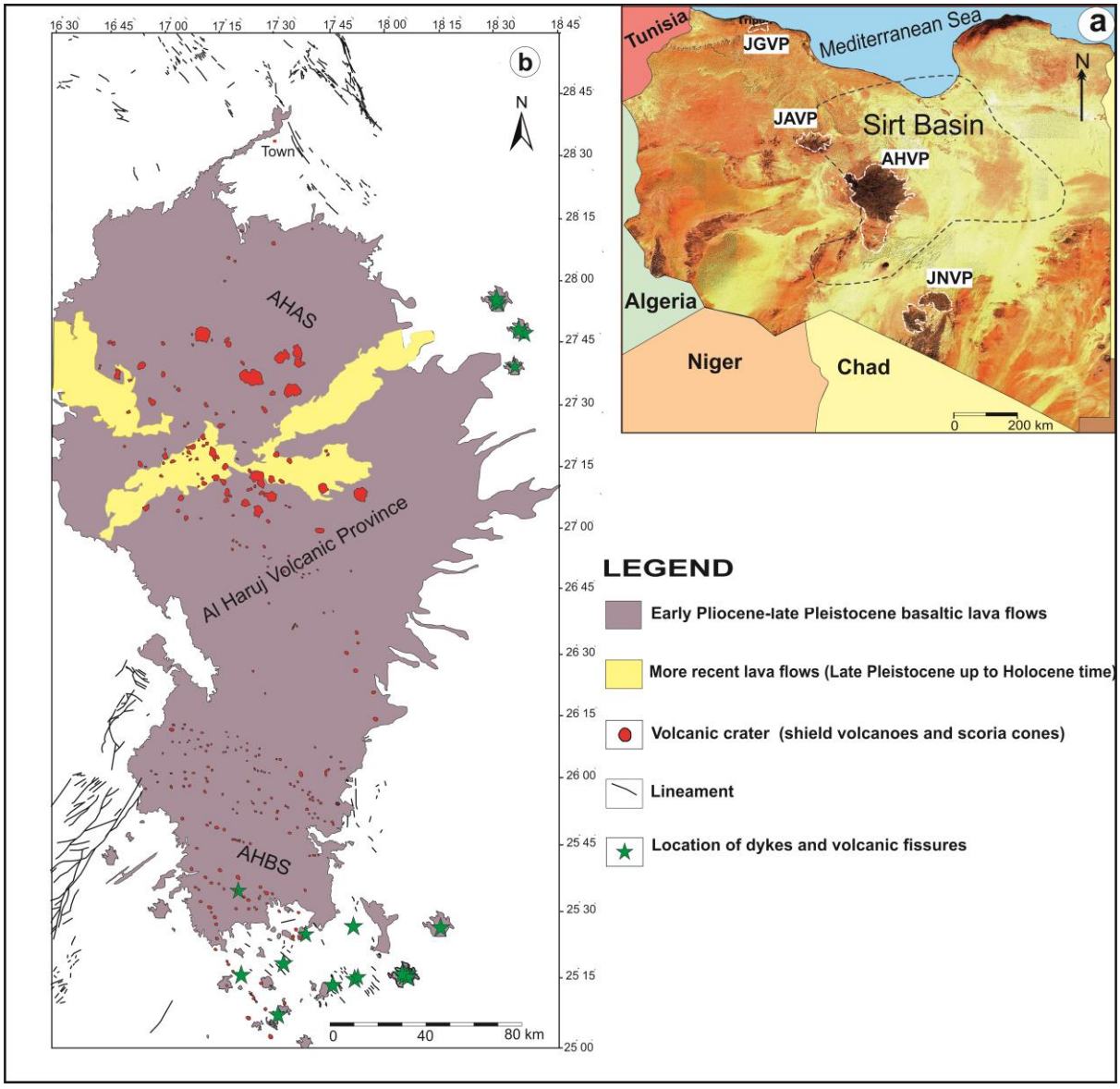

Fig. 1 *a) Satellite image shows the four main occurrence of Tertiary – Quaternary volcanic provinces in Libya which are situated along the axis of the Palaeozoic Tripoli Tibesti Uplift. The Al Haruj volcanic province (AHVP) is located at the south-western margin of the Sirt Basin, central Libya. b) Geological map showing the main structural elements and distribution of eruption points or eruptive centres and more recent lava flows on the Al Haruj volcanic province. Green stars indicate the location of dykes and volcanic fissures. Some of the dykes were mapped by Less et al., (2006). JGVP = Jabal Gharyan Volcanic Province, JAVP = Jabal as Sawda Volcanic Province, JNVP = Jabal Nuqay Volcanic Province, AHAS = Al Haruj al Aswad Subprovince, AHBS = Al Haruj al Abyied Subprovince.*

than Pliocene (Busrewil and Suwesi, 1993; Busrewil, 1996). The other subprovince is located in the south and named the Al Haruj al Abyied Subprovince (AHBS) (the White Mountain). Both subprovinces belong to an area that is slightly prolonged in the NNW-SSE direction (Peregi et al., 2003; Less et al., 2006; Al-Hafdth and El-Shaafi., 2015). The Al Haruj al Aswad Subprovince consists mainly of large lava shields on a lava plateau, while the Al Haruj al Abyied Subprovince consists primarily of clusters of scoria cones and spatter cones, mostly aligned NW-SE (Martin and Nemeth, 2006).

A wide lava plateau was built during the first volcanic phases (early Pliocene), primarily through eruptions of low-viscosity pahoehoe lava flows issued from several hundred volcanic fissures, some of which also generated blocky flows (Busrewil and Suwesi, 1993). Many of volcanic fissures are covered by subsequent lava flows and thus difficult to recognise in the field and on remote-sensing images (Busrewil and Suwesi, 1993; Busrewil, 2012). Many of the topographic features, such as tumuli and lava rises, however, are easily recognised in the field as well as on the aerial photographs and satellite images.

The principal aim of this paper is to present new volcano-tectonic data and models on the AHVP with a view of understanding its volcano-tectonic evolution. The data include feeder-dykes and volcanic fissures, lava shields and pyroclastic (scoria) cones, including their spatial distributions and orientations in relation to the main fault zones in the area. We use the data to estimate magmatic overpressures during fissure eruptions and numerical models to illustrate how some of the dykes may have used steeply dipping normal-fault zones, which are abundant in the area, as part of their paths to the surface.

2 Geological background of the AHVP

The Al Haruj Volcanic Province (AHVP) is located at the south-western margin of the Sirt Basin, one of the main structural elements of North Africa. It follows that the AHVP volcano-tectonic evolution and history is strongly related to the tectonic evolution of the Sirt Basin (Fig. 2). The origin of the volcanism in the Al Haruj province and its volcanic-tectonic evolution are still poorly constrained despite more than five decades of intensive hydrocarbon exploration and the discovery of numerous oil and gas fields in the Sirt Basin.

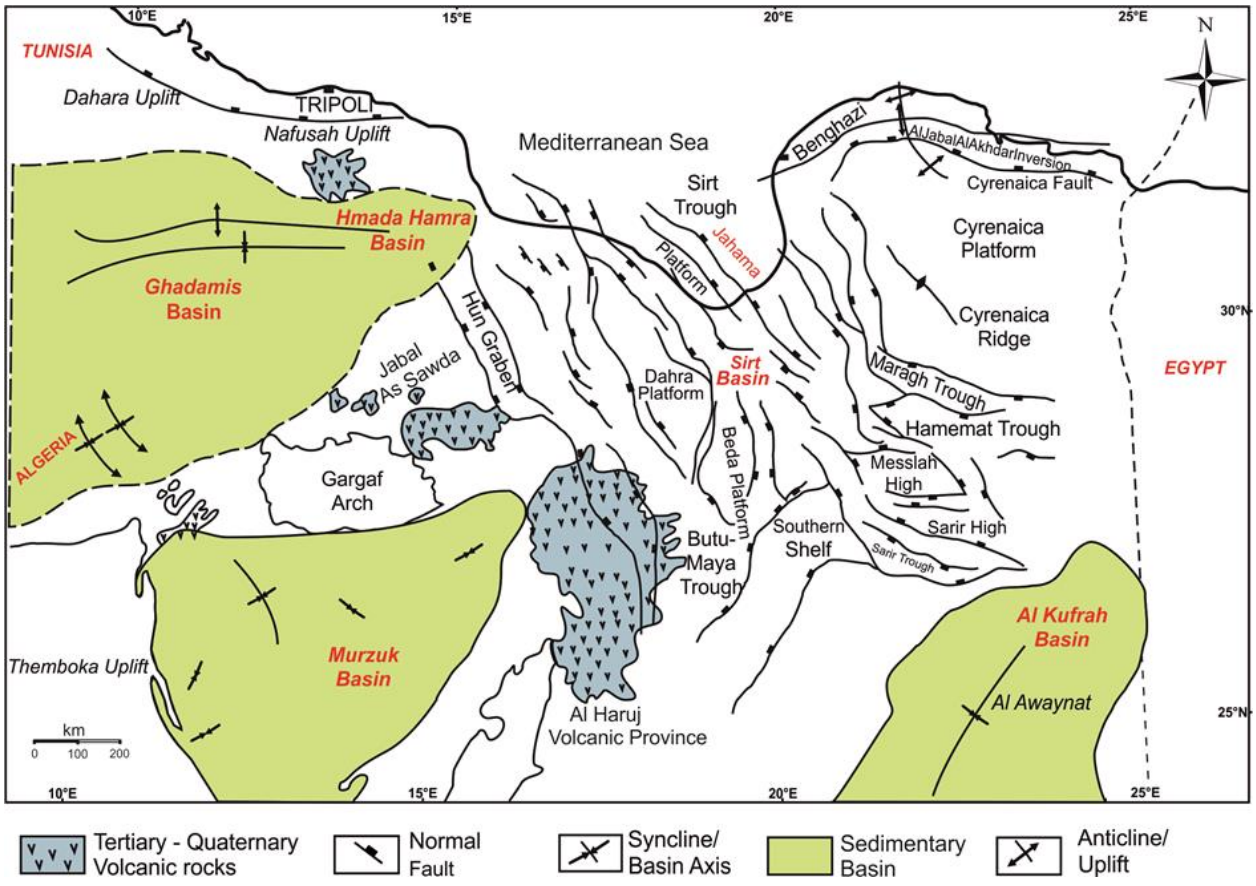

Fig. 2 *Tectonic map showing major structural elements of the Sirt Basin (modified after Mouzughi and Taleb, 1981; Ambrose, 2000; Abadi et al., 2008).*

Many different models have been suggested for the geodynamic setting of the AHVP. Burke (1996) suggests that the Miocene volcanism of Libya was related to the passage of African plate over a relatively fixed asthenosphere hotspot or plume. This is currently not regarded as a very plausible model because (1) the time-related migration of volcanic provinces does not fit well with the movement of the African plate (Farahat et al., 2006; Mohammed, 2014), and (2) peridotite xenoliths indicate a cold lithosphere rather than hotspot at the time of volcanism (Peregi et al., 2003 and Less et al., 2006).

Alternatively, Klitzsch (2000) suggests that the volcanic products of the AHVP relate to relative tensile stresses associated with the reactivation of three major structural elements. These elements are (1) the NW-SE trending Palaeozoic South Al Haruj Uplift, (2) the NE-SW trending Tibesti-Sirt Uplift (Hercynian Orogeny), and (3) the continuation of the Cretaceous – Tertiary Hun Graben (Peregi et al., 2003). In contrast to the other volcanic provinces in Libya, the AHVP is associated with major structural elements that have affected its volcano-tectonic development and may, partly, be the reason for the great size of the AHVP (Farahat et al., 2006).

The primary magmas may have been produced in relation to lithospheric delamination. This is plausible given the rifting of the Sirt Basin since early Cretaceous, inducing low-degree partial melting at depth in the upwelling asthenosphere (Less et al., 2006). Also, the discrete volcanic phases of the AHVP may partly relate to periods of rejuvenation of pre-existing fault system in response to late Tertiary extensional tectonic events most likely related to Africa-Eurasia convergence (Cvetkovic´ et al., 2010). But the time gap between the main syn-rift

phases of the Sirt Basin (late Cretaceous - Eocene) and the volcanism (from early Pliocene to late Pleistocene) is still largely unexplained and debated.

Many authors (i.e. Less et al., 2006) have suggested the magma of the AHVP migrated partly along crustal weaknesses. Yet, the exact process of magma channelling along such weaknesses has not been analysed. Here we explore the role of volcano-tectonics at a crustal scale in the evolution and activity of the AHVP and suggest an alternative mechanism for magma-fault interaction, including new field data and numerical models on volcano-tectonic interactions and stress fields. In particular, we notice and explore several aspects of the activity of the AHVP, including (1) while AHVP covers a large area, the cumulative thickness of the basaltic sequence generally does not exceed 140 m (Pacific Aero Survey, 1979; Peregi et al., 2003), which may indicate low eruption rates (Le Corvec et al., 2013). (2) The magma is generally poorly evolved, indicating lack of significant differentiation stages during magma ascent. (3) Concentrations of major and some trace elements in the eruptive show narrow variations, suggesting magma origin through melting of similar sources and that the magma underwent similar subsequent fractionation processes (Peregi et al., 2003; Less et al., 2006).

3 Geometry and morphology of fractures

The Al Haruj Volcanic Province (AHVP) is thought to have been dominantly extruded from hundreds of feeder-dykes whose surface expressions are volcanic fissures, most of which, however, are covered by more recent lava flows (Busrewil and Suwessi, 1993; Busrewil;

1996). Some of the dykes and volcanic fissures, as well as numerous normal faults, can be seen in the field as well as on Landsat images (Fig. 3).

Field and remote sensing investigations indicate that most of the lineaments in the AHVP are normal faults and extension fractures, some of the extension fractures being volcanic fissures and dykes (Peregi et al., 2003; Less et al., 2006). The geometry and morphology of these lineaments were studied in more detail using ArcGIS 10.1 and multi-source high-resolution remote sensing images for instance the satellite imagery available on Google Earth (2015) for the central part of Libya. Digital elevation model (DEM) and data collected by the NASA Shutter Radar Topography Mission (SRTM) were also used. Google Earth imagery provides three-dimensional geospatial data through Keyhole Mark-up Language (KML). In AHVP, the images are detailed enough so as to provide a resolution of about 2.5 m multispectral at nadir (Abdunaser and McCaffrey, 2014) and allow measurements of the geometries of volcanoes, volcanic fissures, and dykes. The present study confirms that high-resolution remote sensing is an efficient and accurate complementary method to traditional field measurements of lineaments and volcanoes in arid and remote areas (cf. Drury, 2001; Rajesh, 2004; Chen et al., 2014; Abdunaser and McCaffrey, 2014) such the AHVP.

To define the main fracture patterns we analysed the azimuth frequency distributions of lineaments, lineament length and dyke-thickness distributions, as well as lineament densities (Wise et al., 1985; Abebe et al., 1998; Zakir etal., 1999; Francesco and D'Orazio, 2003). The faults and the extension fractures are mainly confined to scattered areas around the main province that range in size from a few to several dozen square kilometres. The bedrocks in these areas are not usually covered with lava flows or Quaternary sand dunes (Fig. 1b).

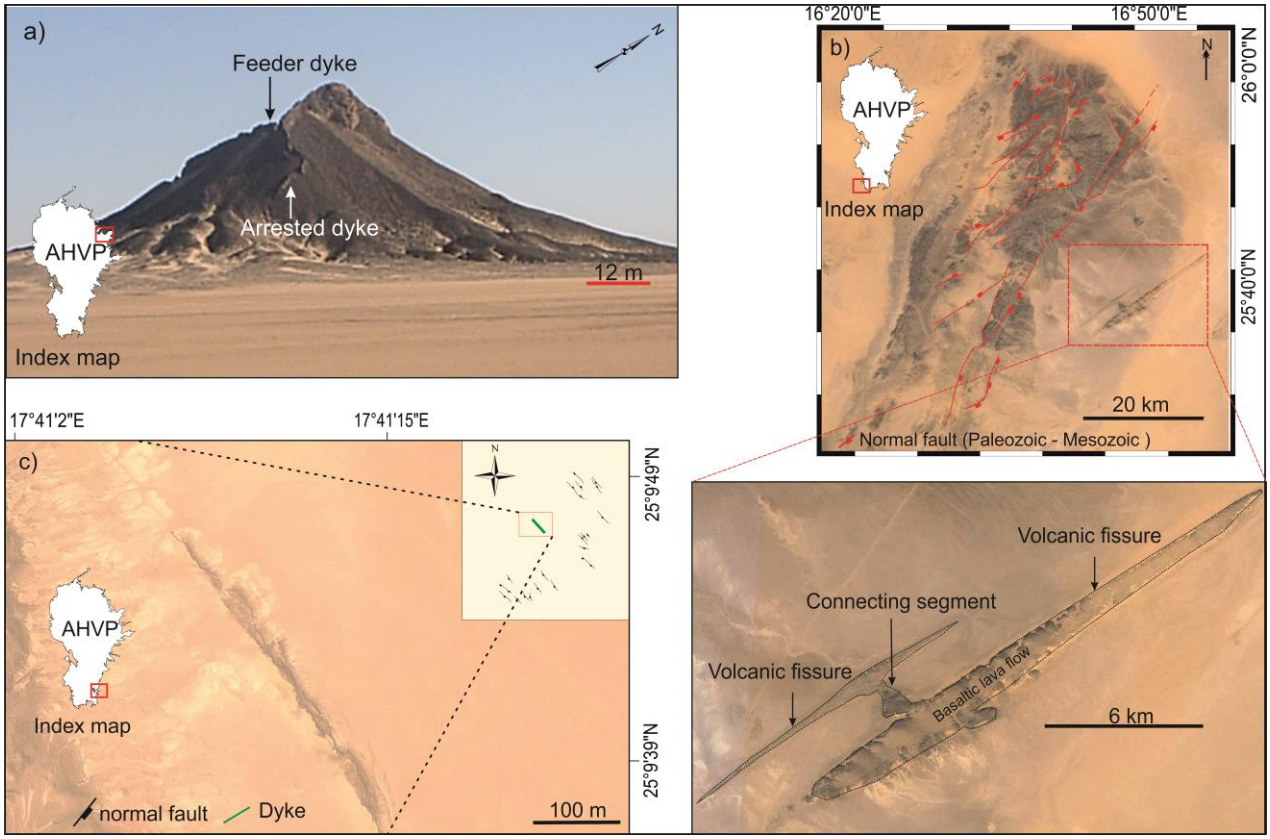

Fig. 3 *a) Field photograph of large ridge (probably volcanic plug or neck) in the north-eastern of the AHVP known as Glyab Al-Baroad that is dissected by several dykes (arrows), which also contribute to the ridge formation. The ridge stands tens of metres above its surroundings, being more resistant to erosion than Miocene host rock (Maradah Formation, calcareous sandstones). The inset map shows the location. b) Landsat images showing two ridges of Dur Qrarat Amhamed in the southernmost part of the AHVP. These are interpreted as volcanic fissures (adapted from Google Earth). Both volcanic ridges constitute long NE-SW trending fissures as well as short WSW-ESE trending connecting segments. Normal faults are taken from Less et al. (2006). c) Segmented dykes are modelled as individual fractures when the nearby tips of the segments are spaced at short distances in relation to the segment lengths. Here the maximum dyke thickness is 0.8 m (adapted from Google Earth). The inset map shows Oligocene-Miocene normal faults. The segments of dykes have similar trend as the faults. Faults were mapped by Less et al. (2006).*

The data are consequently grouped based on types, and then GEOrient software was used to plot the directions of fissures, dykes, and faults on rose diagrams.

4 Extension fractures

The only published studies on volcanic fissures and dykes in the Al Haruj volcanic province are those by Less et al. (2006). The dykes strike mainly from NW-SE to NNW-SSE, directions which are generally parallel to the strike of major faults in the Sirt Basin and similar to the trend of inferred and observed volcanic fissures. A minor dyke trend, from NNE-SSW to NE-SW, may be related to inheritance of Palaeozoic crustal weaknesses (Less et al., 2006).

The thicknesses of the dyke segments are commonly 0.5 - 2 m thick (Fig. 4), while some may be as thick as 20 m, and their lengths are mostly 0.1-1km (Less et al., 2006). These figures are similar to those of regional dykes in many other volcanic areas (Gudmundsson, 1995; Babiker and Gudmundsson, 2004). Some dykes in the eastern and southwestern part of the AHVP form ridges (Fig. 3a, b). All dykes and volcanic fissures, as seen in the field and on satellite images, are segmented. Such segmented extension fractures, however, are normally modelled as single fractures or cracks when the nearby ends of the segments are separated by less than 10% of the segment lengths, in which case the segments act mechanically essentially as a continuous fractures (Fig. 3c; Gudmundsson, 2011a). Remote sensing images have been used to extract length, thickness, and strike of 47 dyke segments and volcanic fissures around margins of the Al Haruj volcanic province (Table 1, Appendix I), all

parameters that are important when considering the mechanics of dyke emplacement and associated stress fields (Babiker and Gudmundsson, 2004). The relation between lengths and

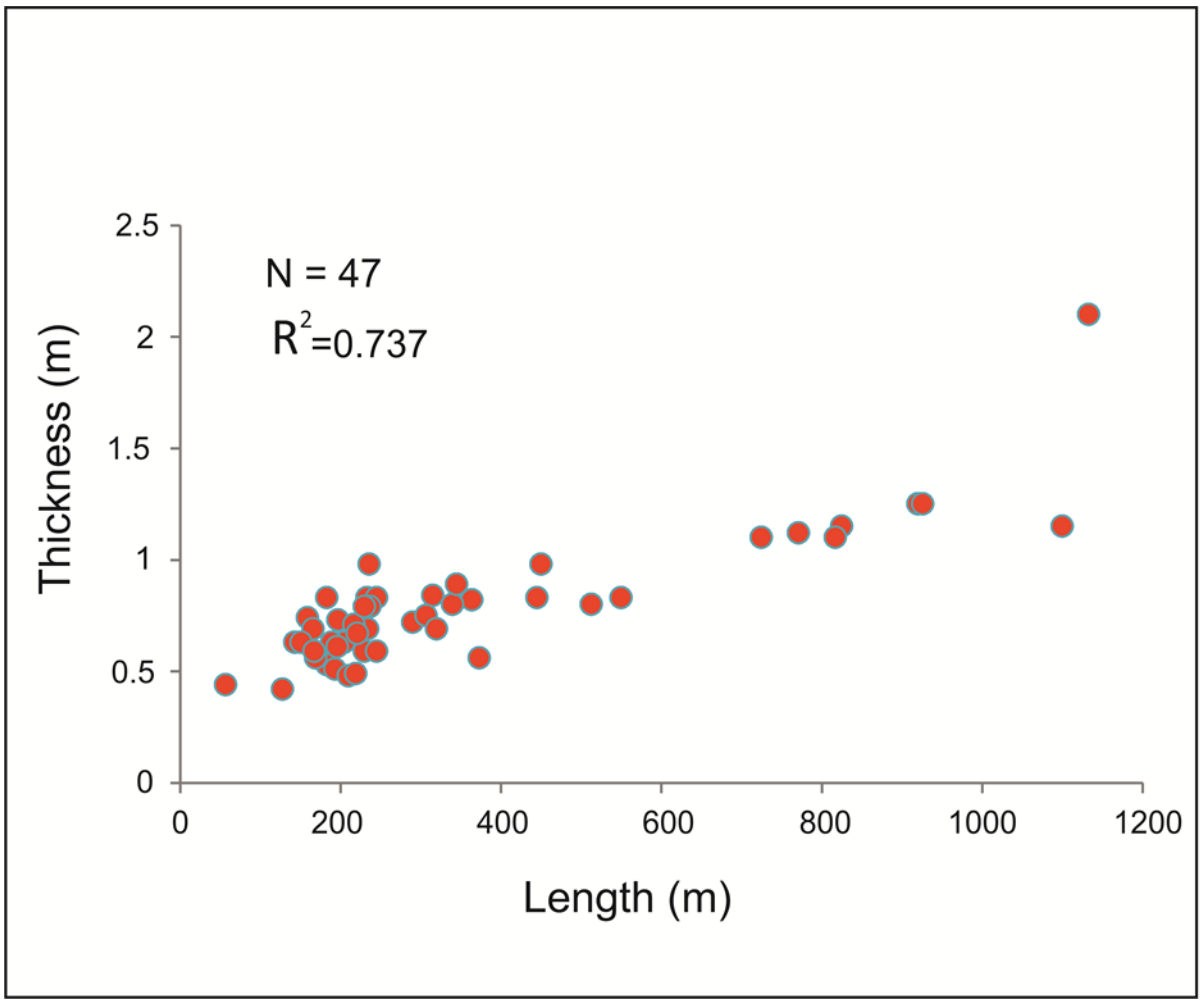

Fig. 4 *Diagram showing a roughly linear correlation between length and thickness of 47 dyke segments and volcanic fissures on the AHVP. R^2 is the coefficient of determination.*

thicknesses of these extension fractures is roughly linear (Fig. 4.), in agreement with standard fracture-mechanics theory (Gudmundsson, 2011a).

4.1 Magmatic overpressure of the Al Haruj Volcanic Province

A magma chamber ruptures and injects a dyke when the conditions of Eq. (1) are met at any location in the walls or roof of the chamber, regardless the shape of the chamber (Browning et al., 2015):

$$p_l + p_e = \sigma_3 + T_0 \quad (1)$$

where p_e is the excess magmatic pressure in the chamber at the time of rupture, that is, the difference between the total magma pressure p_t and lithostatic stress p_l, and σ_3 and T_0 are the minimum compressive (maximum tensile) principal stress and the in situ tensile strength of the chamber host rock, respectively. As the dyke begins to propagate up into the roof of the chamber, the magma overpressure in the dyke becomes:

$$p_o = p_e + (\rho_r - \rho_m)gh + \sigma_d \quad (2)$$

where ρ_r is the host-rock density, ρ_m is the magma density, g is acceleration due to gravity, h is the dip dimension and σ_d is the differential stress at the level where the dyke is observed for a feeder-dyke (volcanic fissure) at the surface (Gudmundsson, 1990; Gudmundsson, 2011a).

The magmatic overpressure p_0 measures the difference between the total magma pressure and the minimum principal compressive stress σ_3, which acts normal to the dyke; p_0

increases up along the dyke fracture so long as the buoyancy term $(\rho_r - \rho_m)gh$ is positive. During fissure eruptions, the overpressure p_0 has large effects on the volumetric flow or effusion rate (Gudmundsson, 1990; Gudmundsson, 2011a; Kusumoto et al., 2013).

From the aspect (strike dimension/thickness) ratio of the dyke, its overpressure p_0 at the time of its formation can be calculated. The following equation supposes the magmatic overpressure is constant, which is a good first approximation generally and particularly when there is limited data as to the exact thickness variations of dykes and volcanic fissures (Becerril et al., 2013):

$$p_o = \frac{\Delta u E}{2L(1-\nu^2)} \tag{3}$$

Here ν is Poisson's ratio of the host rock, E its Young's modulus, Δu the maximum aperture or thickness of the dyke, and L the strike dimension (horizontal length) of the dyke. Dykes are primarily extension fractures that are modelled as either through cracks (when feeders) or part-through cracks (when arrested). In particular, feeder-dykes extend from one free surface (the source magma chamber) to another one, namely the Earth's surface (Fig. 5; cf. Gudmundsson, 2011a). Non-feeders propagate from one free surface (the source magma chamber) and then become arrested at some depth below the surface, usually at contacts between mechanically dissimilar layers (Gudmundsson, 2011b).

Lengths of measured dykes and volcanic fissures at AHVP range from 57m to 1133m and their thicknesses or openings (palaeo-apertures) from 0.42 to 2.1m (Appendix I).

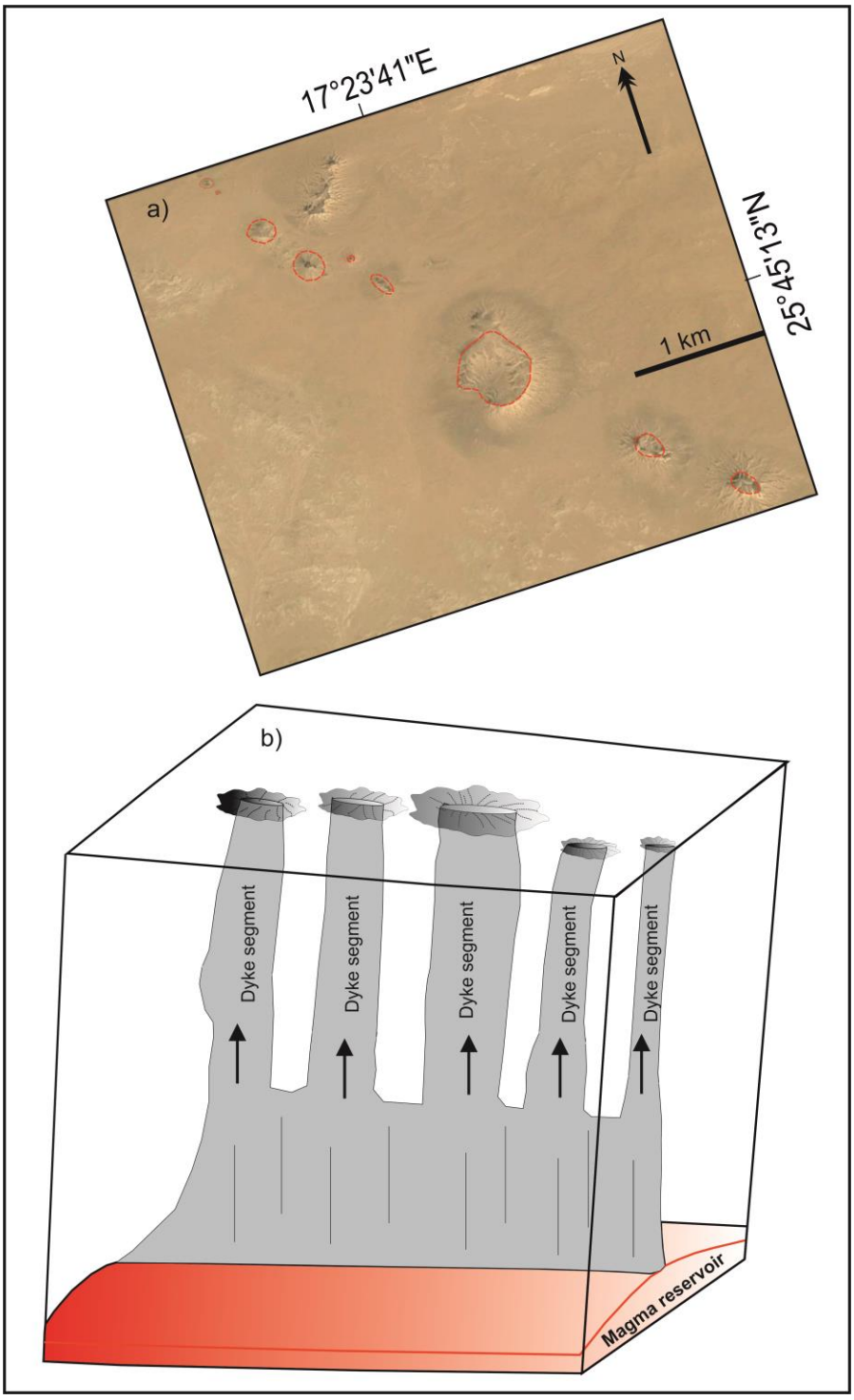

Fig. 5 *a) Image showing several eruption points/centres fed by a segmented dyke (adapted from Google Earth). b) Schematic illustration of a segmented dyke, the segments being extension fractures (mode I cracks). When the dyke, as here, extends from one free surface (magma chamber) to another free surface (Earth's surface), it is modelled as a through crack. The dyke length or strike dimension is smaller than the height or dip dimension. Therefore, the strike dimension is the controlling dimension (modified after Gudmundsson, 2011a).*

The estimated uncertainties or errors in the measurements are 5% for length and 15% for thickness. Most of the dykes and fissures strike NW-SE. The average aspect (length or strike dimension/thickness) ratio is 421, which is within a factor of 2 for aspect ratio estimates from other areas (Becerril et al., 2013). The aspect ratio depends much on the stiffness or Young's modulus of the host rocks where the dykes/fissures are measured.

The static Young modulus (E) of the uppermost crust of the Sirt Basin, based on drill-core samples, is estimated in the range of 8 - 20GPa (Qui et al., 2008). The basement rocks in the south western portion of the Sirt Basin are mostly granodiorite, granite, and metamorphic rocks and overlain by around 2000 m of various types of sedimentary rocks. The in-situ Young's modulus is likely to be lower than the core-sample modulus (Gudmundsson, 2011a) and is here assumed in the range of 7 - 15GPa. Poisson's ratio ν of most rocks is in the range 0.2 - 0.3; we use the typical average value of 0.25 (Gudmundsson, 2011a), which is similar to ν values obtained in laboratory tests on core samples in the Sirt Basin (Qiu et al., 2008). We assume the strike dimension (outcrop length) to be the controlling dimension, that is, smaller than the dip dimension (depth to the source magma chamber). This follows because the depths to the magma chambers (the dip dimension) in the AHVP is estimated at 35 - 55km (Peregi et al., 2003), many times larger than the measured strike dimensions of the dykes.

From Eq. (3), using the measured aspect ratios and inferred elastic properties of the host rock, the magmatic overpressure of individual dykes can be estimated. For the average aspect ratio, magmatic overpressure is from 8MPa (E = 7GPa) to 19MPa (E = 15). These results are very reasonable. The lower value (8MPa) is similar to those obtained in many other studies from different volcanic provinces (Delaney and Pollard, 1981; Poland et al., 2008; Geshi et al.,

2010; Kusumoto et al., 2013) and is close to the maximum in-situ tensile strength of rocks (Gudmundsson, 2011a; Kusumoto et al., 2013). The higher value (19MPa) is similar to those obtained in areas where, like in the AHVP, the depth of origin of the basaltic magma forming the dykes is great (Becerril et al., 2013).

5 Magma propagation from the source chamber

Nearly all eruptions are fed by dykes and inclined sheets. Understanding the mechanics of dyke emplacement and propagation through the Earth's crust (e.g., Gudmundsson et al., 2014) is therefore crucial for a better understanding of volcano-tectonic processes in general and those operating in the AHVP in particular. Dykes occur mainly in elongated swarms outside the main volcanic system, whereas the shield volcanoes and scoria cones are mostly confined to the northern, central as well as the southernmost of this province (Fig. 1b).

While the Al Haruj area is located within the most important hydrocarbon sedimentary basin in Africa, the details of the geometry of sills, dykes, and inclined sheets that eventually fed the eruptions are still poorly understood. In the past few years, many models on intrusions in sedimentary basins have been developed, focusing mostly on sill emplacement (Planke et al. 2005; Cartwright and Hansen 2006; Polteau et al. 2008; Thomson and Schofield 2008; Gudmundsson and Lotveit, 2012; Holt et al., 2014). Sills can propagate laterally within basins for tens or hundreds of kilometres and attain various shapes (Cartwright and Hansen, 2006; Hansen and Cartwright, 2006; Gudmundsson and Lotveit, 2012; Barnett and Gudmundsson, 2014). However, magma transport to the surface is mostly through dykes, and

outside central volcanoes (where inclined sheets are common) almost exclusively so. Here we therefore focus on dyke propagation.

5.1 Mechanics controlling the propagation of dyke

When a dyke injected from a source magma chamber meets a discontinuity such as a contact, it can respond in one of four ways: (a) become arrested at the contact, (b) penetrate the contact and continue its propagation towards the surface (perhaps eventually erupting), and (c) change into sill through and single deflection or (d) double deflection along the contact (Gudmundsson, 2011b; Barnett and Gudmundsson, 2014). Arrest or deflection of a dyke at a contact is controlled by three main mechanisms, namely:

a) Stress barriers (layers where the principals stresses have rotated so as to become unfavourable for dyke propagation)

b) The Cook-Gordon debonding or delamination (induced dyke-parallel tensile stress opens the contact ahead of the propagating dyke tip)

c) Elastic mismatch (relates to change in Young's modulus across a contact in relation to the contact properties and material toughness)

Several numerical models on dyke deflection and arrest were made using Comsol Multiphysics (5.1) (www.comsol.com), a finite element (FEM) software package for various physics and engineering applications (Tabatabaian, 2014). The dykes are modelled as elliptical holes subject to constant magmatic overpressure of 10 MPa (the typical value based on the above range of 8 - 19 MPa estimated above). The vertical dimension or height of the

model is taken as a unit and all the layers have the same Poisson's ratio, 0.25, and density, 2500 kg/m^3. The models are fastened at the edges to avoid rigid-body rotation and translation. The direction of dyke propagation is inferred from the trajectories or ticks showing the direction of the maximum principal compressive stress σ_1. The contours of the calculated maximum principal tensile stress, σ_3, are also shown.

For a homogeneous and isotropic crust, so long as there is magmatic overpressure in the dyke it should reach the surface as a feeder (Gudmundsson, 2011a). Field observations, however, show that most dykes become arrested at contacts between layers in anisotropic (layered) crustal segments (Gudmundsson, 2011b; Browning and Gudmundsson, 2015) and are thus non-feeder dykes. The dykes may stop altogether at the contacts, or change into sills – which have the potential of developing into shallow magma chambers. Our numerical models illustrate how arrest can occur in relation to the three main arrest conditions indicated above, which we now discuss in more detail.

5.1.1 Stress barrier (the rotation of the principal stresses at the contact between layers)

This mechanism operates when a dyke meets a layer with local stress field that is unfavourable to dyke propagation (Barnett and Gudmundsson, 2014; Tibaldi, 2015); namely, the maximum compressive principal stress field σ_1 is rotated 90^o so as to become horizontal. Examples include contact where across which Young's modulus changes abruptly (Fig. 6). Stress barrier thus partly control the frequency with which injected dykes reach the surface to feed eruptions (Gudmundsson et al., 2010).

5.1.2 Cook-Gorden debonding mechanism

The dyke-parallel tensile stress induced ahead of propagating dyke is about 20% of the induced tensile stress of perpendicular to the dyke (Fig. 7a) and can open up contact ahead of dyke tip if it reaches the tensile strength T_0 of the contact (0.5 - 9MPa and most commonly 2 - 5MPa; Gudmundsson, 2011a). On meeting the open contact then, depending on the magmatic overpressure, the dyke either becomes arrested or changes into a sill (Barnett and Gudmundsson, 2014) (Fig. 7b, c).

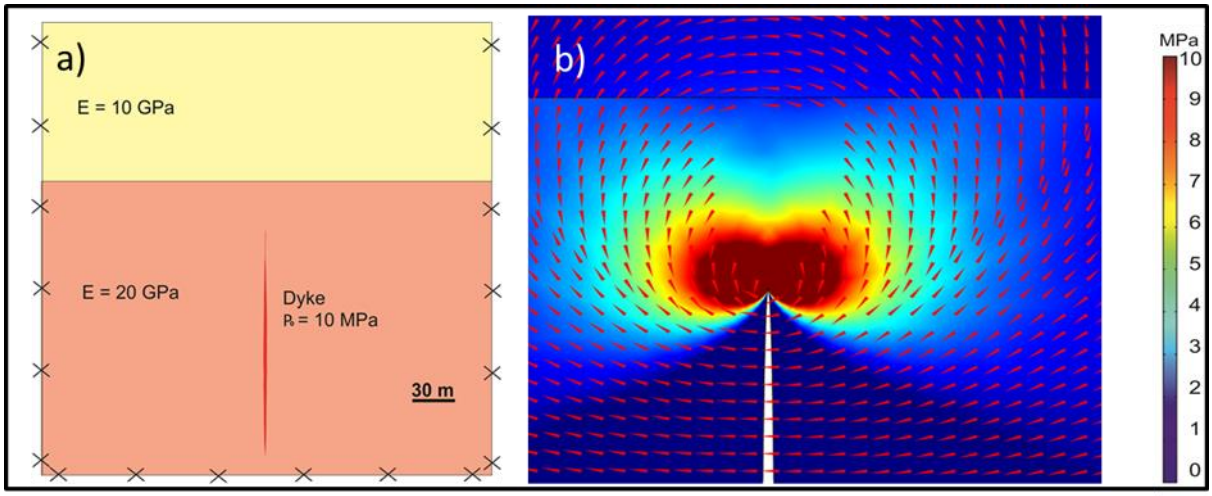

Fig. 6 *a) Model setup of two layers with different mechanical properties, the lower layer hosting a dyke. b) Numerical model results showing the stress trajectories of the maximum principal compressive stress* σ_1 *represented by red arrows, while the colour contours represent maximum principal tensile stress* σ_3*. This model and subsequent models are fixed at the sides, indicated by crosses, to avoid rigid body rotation and translation.*

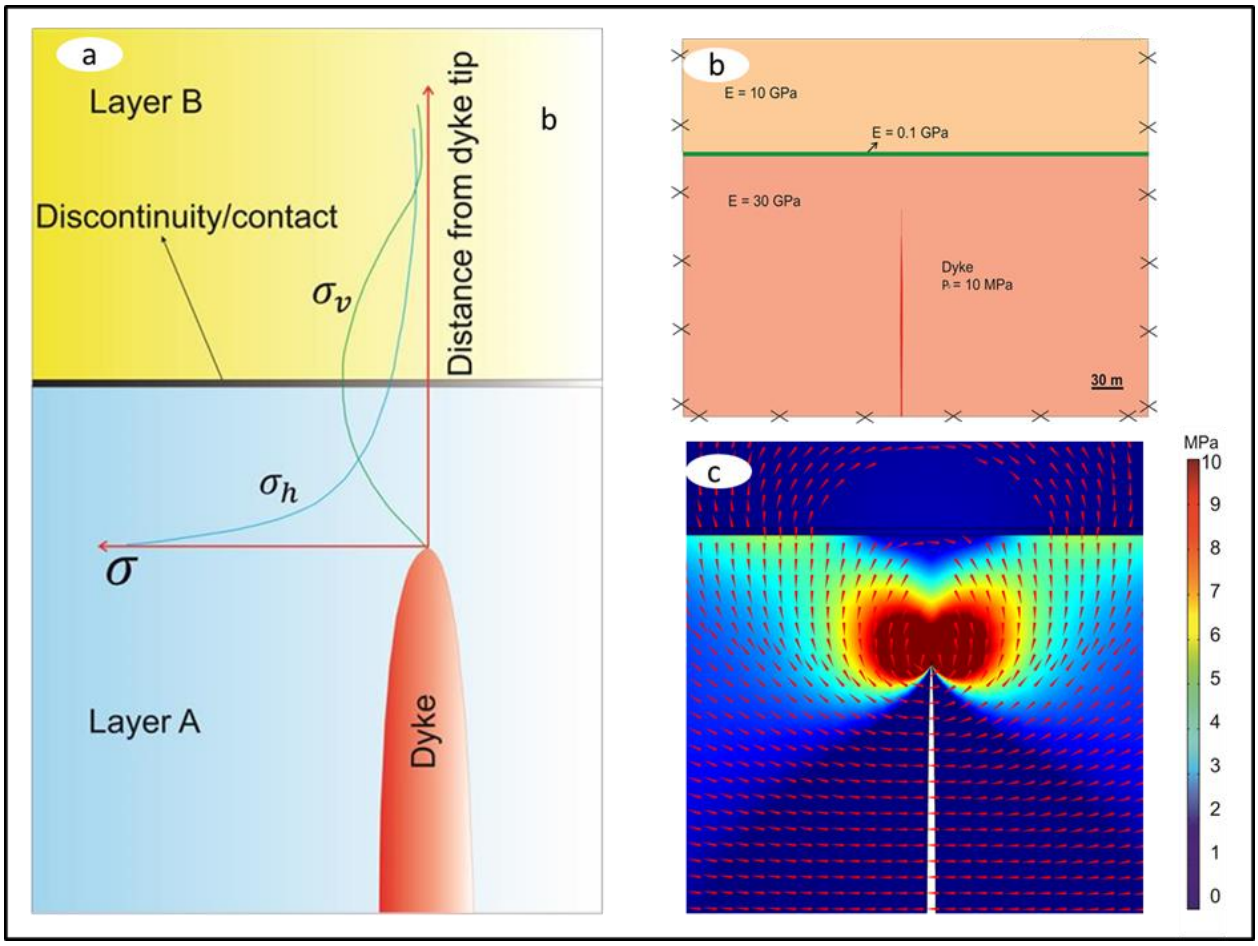

Fig. 7 *a) The dyke-parallel tensile stress at the head of propagating dyke is about 20% of the tensile stress perpendicular to the dyke and may open up a weak (low tensile-strength) contact or discontinuity at ahead of the dyke. This is known as Cook-Gordon debonding or delamination mechanism (modified after Thouless and Parmigiani, 2007; cf. Gudmundsson, 2011a). b) A weak contact (green) is modelled as soft thin layer that is located between two stiffer layers. c) Model results showing rotated ticks (trajectories) of* σ_1. *When a dyke reaches this contact the dyke may become arrested or deflected along the contact depending on magmatic overpressure of the dyke, the contact strength, and the magnitudes of the principal stresses.*

5.1.3 Elastic mismatch

This mechanism operates when there is an abrupt change in the elastic properties, particularly in Young's modulus, across a contact (cf. He and Hutchinson, 1989). More specifically, when a dyke meets a contract, the ratio of strain energy release rate (a measure of material toughness or resistance to fracture) for dyke deflection (into a sill) along the contact G_d to that of dyke penetration G_p, both in relation to Dundurs elastic mismatch parameter, α (Fig. 8; Gudmundsson, 2011a,b) may control what happens to the dyke.

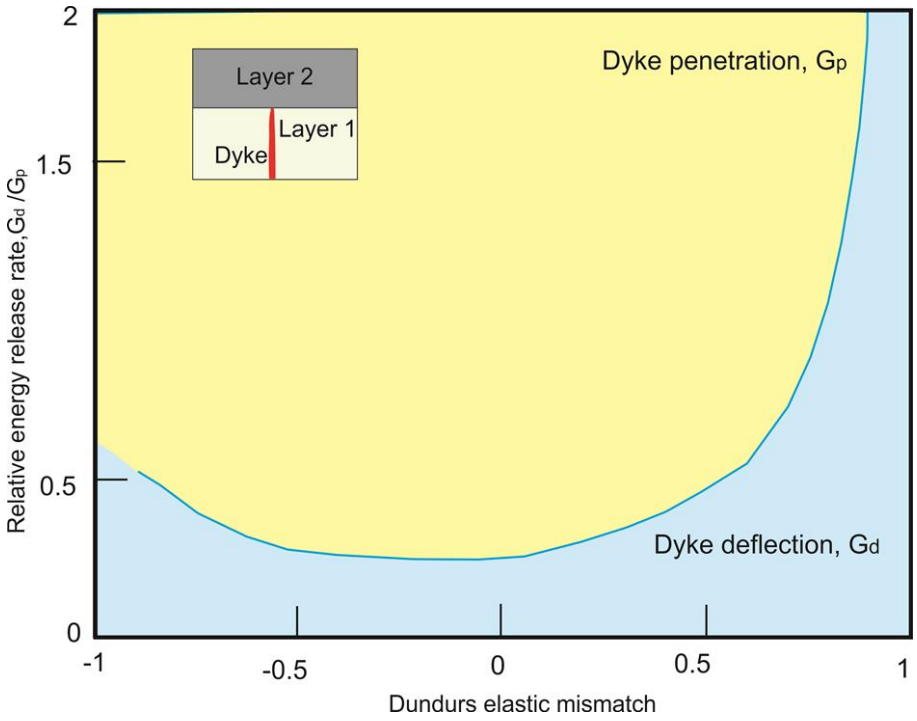

Fig. 8 *Schematic illustration of the mechanism of elastic mismatch and material toughness for deflection or penetration of a dyke when it meets a contact. Dyke penetration mainly occurs when Dundurs elastic mismatch across the contact equals zero. The Dundurs parameter becomes negative when the layer hosting the dyke (layer 1) is stiffer than the layer above the contact (layer 2), whereby the dyke has a little propensity to deflection into a sill along the contact. Alternatively, when the Dundurs parameter becomes positive the dyke has great tendency to deflect into sill along the contact (modified after He and Hutchinson, 1989; Hutchinson, 1996).*

There is little difference in the elastic strain energy release rate for a single or double deflection. For negative values of Dundurs elastic mismatch parameter, layer 1 (the dyke-hosting layer) is stiffer than layer 2 and there is little tendency to dyke deflection along the contact. However, as the stiffness of layer 1 increases in relation to that of layer 2, the tendency to dyke deflection along the contact greatly increases. If there is no Young's modulus mismatch across the contact dyke deflection occurs only if contact material toughness is about 26% of the toughness of the rock on the other side of the contact. When the elastic mismatch increases (to the right), however, dyke deflection will occur even the contact toughness becomes equal to and higher than the toughness of layer 1.

6 Spatial density of volcanic eruptions

The spatial distributions of 432 volcanic eruptions points (monogenetic volcanoes) were examined and are presented on a density map (Fig. 9). ArcGlobe 10.1 was utilised to plot the volcanic vents, with the shape files of volcanoes imported into ArcMap10.1. The density map calculates the frequency of eruption points or eruptive centres that fall within a neighbourhood around each raster cell. A neighbourhood is defined around each cell centre, and then the cumulative number of eruption points/centres is divided by the area of the neighbourhood.

The spatial density map is drawn by ArcGIS 10.1 for a search radius of 40 km, producing a generalised output raster (Lesti et al., 2008), gives the volcano distribution and density variation in the area. Fractures were added to the map through georeferenced raster images of the geological maps of the AHVP as a guide.

Only volcanoes with clear boundaries were compiled, the main types being lava shields, pyroclastic or scoria cones, and (a few) maars. The volcanic points are clearly clustered (Fig. 9), and some are associated with volcanic fissures. There are two main density subzones. The first occurs in the northern part of the AHVP and is mainly composed of large lava shields and some scoria cones – these constitute the most recent eruption sites in the area. The second occurs in the southern part of the AHVP and is primarily composed of scoria cones, with comparatively few lava shields, yielding smaller eruptions, on average, than in the northern cluster. The lowest frequency of eruption points/centres occurs in the central area between the northern and the southern cluster (Fig. 9). The volcanic fissures (lineaments) are primary WNW-trending, coinciding with the general trend of the main volcanic zone/crustal weakness/fracture zone in the area.

7 Spatial alignment of volcanic eruptions

The volcanic fissures were obtained through alignments of volcanic points (Fig. 10). When more than one possible alignment could be made, elongate craters are used as an indication of the general trend and the vents along that trend are joined, following a standard method (Paulsen and Wilson, 2009). The strike of the aligned vents is then assumed to coincide with that of a volcanic fissure/feeder-dyke when more recent flows cover part of the fissure.

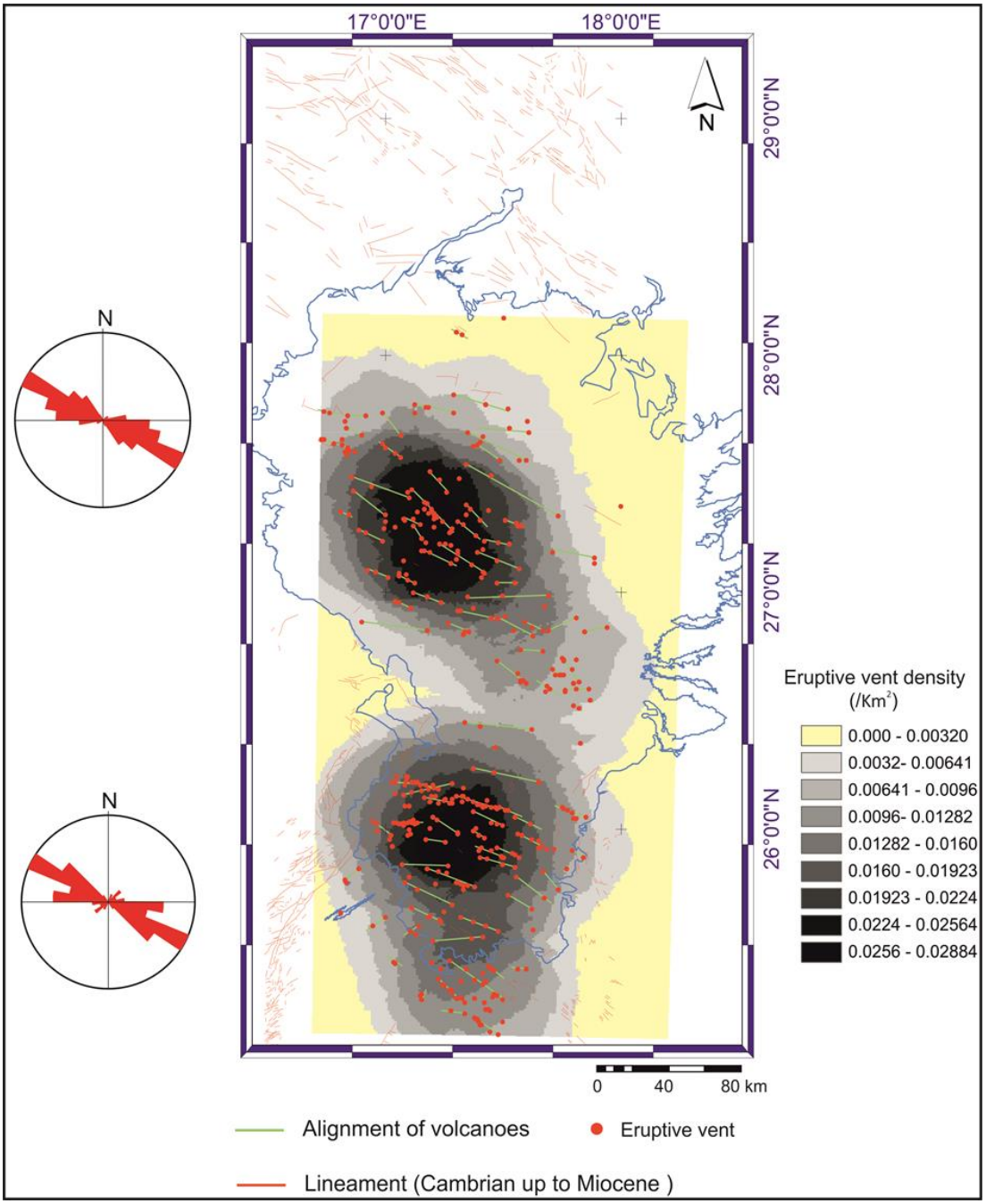

Fig. 9 *Density map of the volcanoes of the AHVP. In total 432 eruption points/centres were mapped in this study, most of which are lava shields (small monogentic shield volcanoes) and pyroclastic (scoria) cones. Spatial alignments of the volcanoes, as inferred from satellite imagery, and their trends are plotted in rose diagrams for each density maximum zone. The locations of the lineaments are taken from Busrewil and Suwesi, (1993), Peregi et al. (2003), Less et al. (2006), and Abdunaser and McCaffrey (2014).*

The rose diagrams for the strike of volcanic fissures, made using the GEOrient software, show that WNW-ESE trends dominate, with small NE-SW subsets. Rose diagrams for some 1000 (mostly normal) faults, extension fractures and alignments of volcanoes in the area show two main sets (Fig. 11 a,b,c). One set strikes WNW-ESE, while other set of strikes between NE and ENE, which is similar to that of some of the large volcanic ridges in the area (Fig. 3 a,b). The length-size distribution of these fractures are roughly log-normal, as is common for fractures (Fig. 11 a,b,c; Babiker and Gudmundsson, 2004).

8 Structural evolution of the Al Haruj Volcanic Province

The tectonic evolution of the AHVP may be divided into five main deformation episodes or phases (Peregi et al., 2003), each of which is characterised by structural elements that differ in orientation (and thus in associated stress fields) and timing from the elements of other phases (Appendix II). The main structural features in the area relate to Phase IV and V, which occurred during Palaeogene–Quaternary and can be linked to the most recent evolution of the Sirt Basin (Cvetkovic et al., 2010). In particular, during phase IV most of the Al Haruj region was subject to NE-SW oriented tension, roughly perpendicular to main structural elements in the northern and central parts of the area (Less et al., 2006). Similarly trending structural elements have been identified in the central and western parts of the Sirt Basin (Anketell, 1996; Abadi et al., 2008; Abdunaser and McCaffrey, 2015).

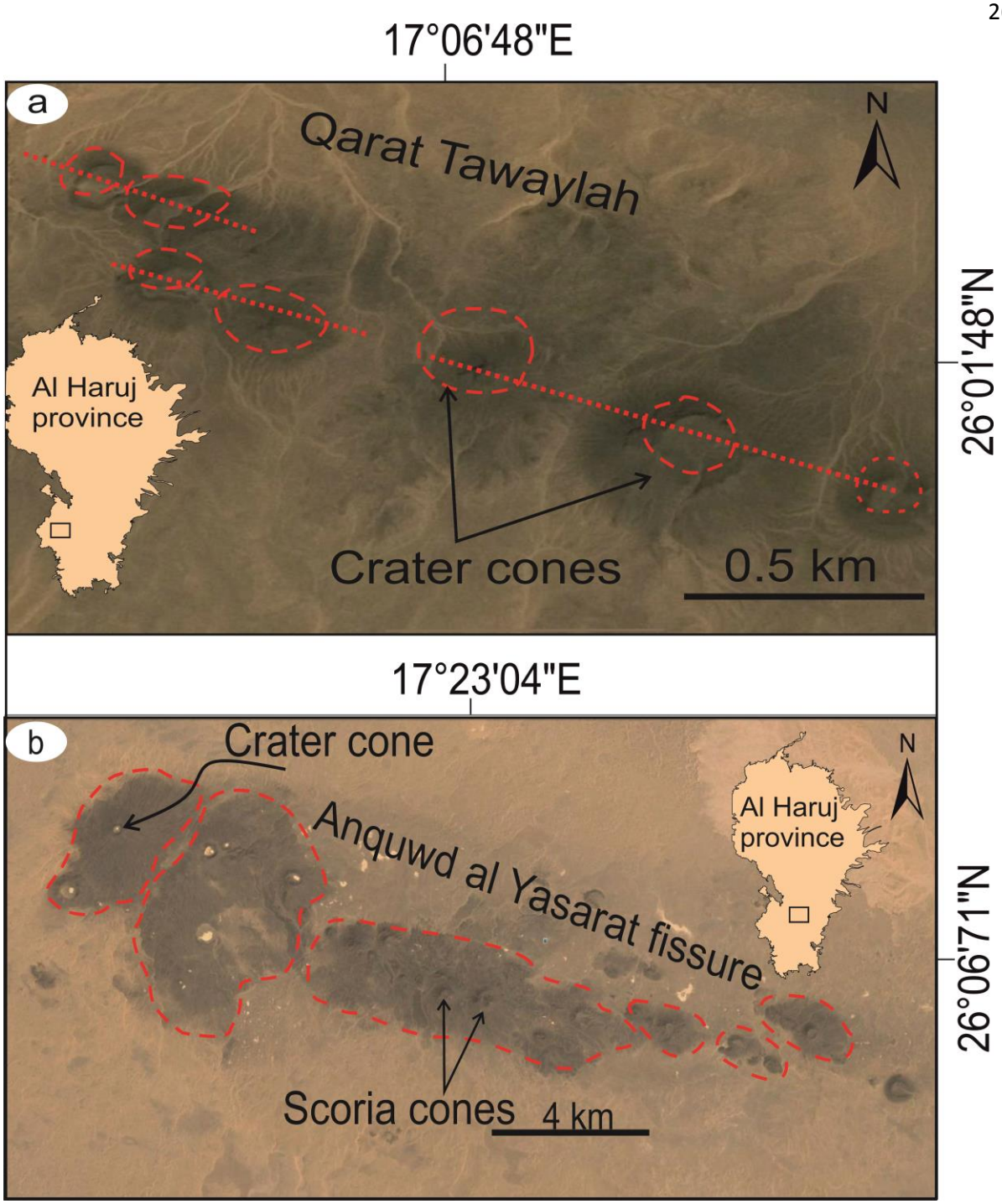

Fig. 10 *Satellite images (adapted from Google Earth) showing examples of spatial alignment of volcanic eruption points/centres in the southern portion of the AHVP. a) NW-SE trending alignments of volcanoes. The long axes of the craters and alignments mark the strike orientation the subsurface feeder-dykes (cf. Paulsen and Wilson, 2009). b) WNW-ESE trend inferred from several pyroclastic/scoria cones. The inset maps provided the location.*

In contrast to the local stress field of the AHVP, the regional stress field for the whole area, including the Sirt Basin, relates to NW-SE compression and NE-SW extension (Appendix III; Less et al., 2006). Abdunaser and McCaffrey (2015) inferred from 2D seismic lines and borehole data that the structure of the south-western part of the Sirt Basin is primarily composed of high-angle normal faults striking NNW-SSE and related to late Cretaceous to Eocene extensional tectonics superimposed on inherited Pan-African basement structures (early Palaeozoic) and pre-existing Hercynian structures (late Palaeozoic- early Mesozoic) (Fig. 12). Pre-existing structural elements are likely to have affected the volcanic activity in the AHVP, to which we turn now.

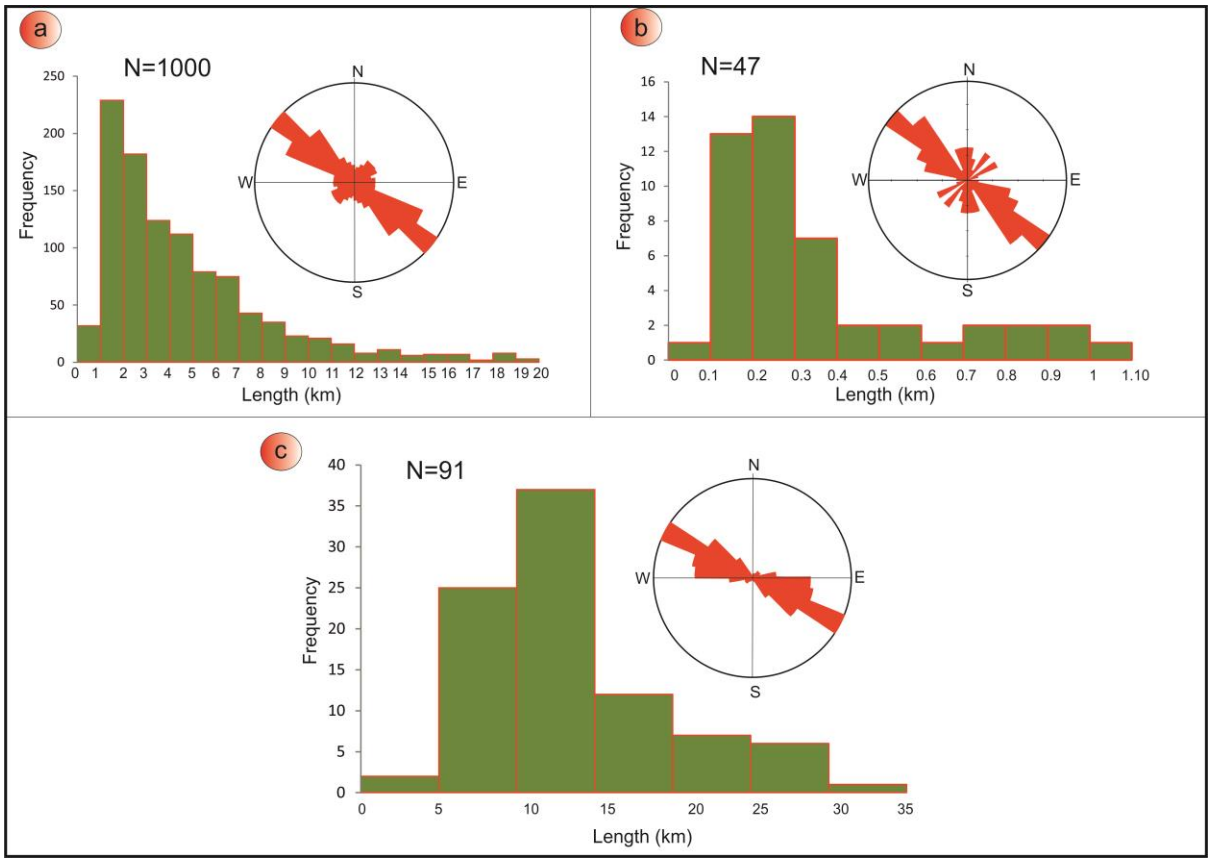

Fig. 11 *Rose diagrams and frequency distributions of a) 1000 faults (mostly normal faults) mapped from available geological maps of the Al Haruj region, b) 47 dykes and volcanic fissures, c) 91 alignment of eruption points/centres. Length-size distributions of these lineaments are roughly lognormal.*

9 Discussion

9.1 Role of pre-existing fracture zones in providing magma paths

One principal question that arises is why and how magma reaches the surface in the AHVP, and what the relation is, if any, between the volcanic activity in AHVP and the tectonic activity in the nearby Sirt Basin. Here we discuss the interaction between faults and dykes, both with reference to earlier data and models as well as our own results.

During the last two decades a substantial amount of deep hydrocarbon wells have been drilled throughout the Sirt Basin. Using these data, Busrewil et al. (2012) suggest that the Cretaceous basaltic rocks (100 - 130Ma) within the Nubain clastics in Al Hameimat trough, NE Sirt Basin, were fed by dykes that may partly have used high angle normal faults as paths (Fig. 13). It is well known that dykes use pre-existing structures, primarily joints but sometimes high-angle (primarily normal) faults, to form their paths (Delaney et al., 1986; Gudmundsson, 2011a; Gudmundsson et al., 2010; Magee et al., 2013; Bedard et al., 2012; Tibaldi, 2015), so the idea is worth analysing.

Fault zones are composed of two main mechanical units or zones, a fault core and a fault damage zone (Fig. 14). In large fault zones the damage zone may reach thickness of up to a few kilometres, but is more commonly of the order of tens to hundreds of metres (Gudmundsson et al., 2010). The damage zone may contain breccia, but is characterised by fractures whose frequency varies (mostly irregularly) with distance from the core.

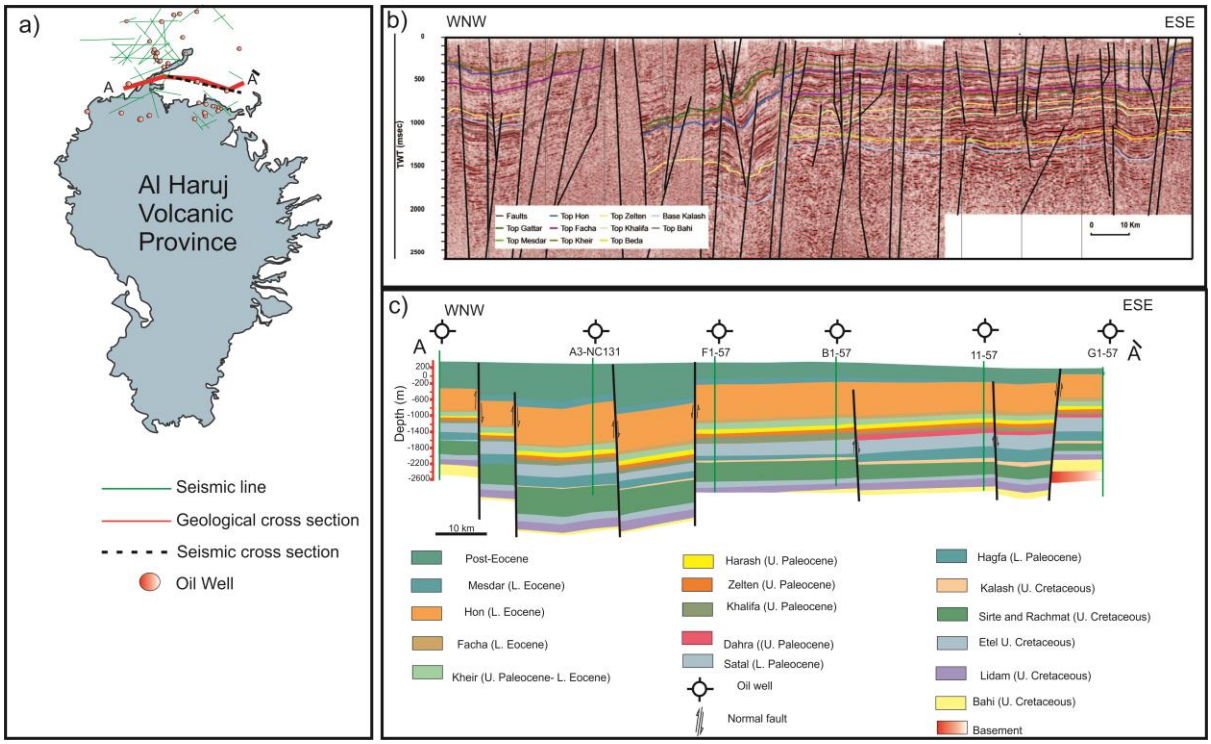

Fig. 12 *a) Location of oil wells, seismic lines, and cross-sections in the northernmost of the AHVP. b) Seismic section, most of these high-angle normal faults (Abdunaser and McCarffrey, 2015). c). Geological cross section inferred from borehole data (modified from Abdunaser and McCarffrey, 2015).*

By contrast, the core, commonly several metres thick in major fault zones, consists primarily of gouge and breccia. The boundary between damage zone and host rock vary along the fault and change spatially and temporarily with the evolution of the fault zone in active fault whereas in inactive faults the contact between them is generally sharp (Gudmundsson, 2011a).

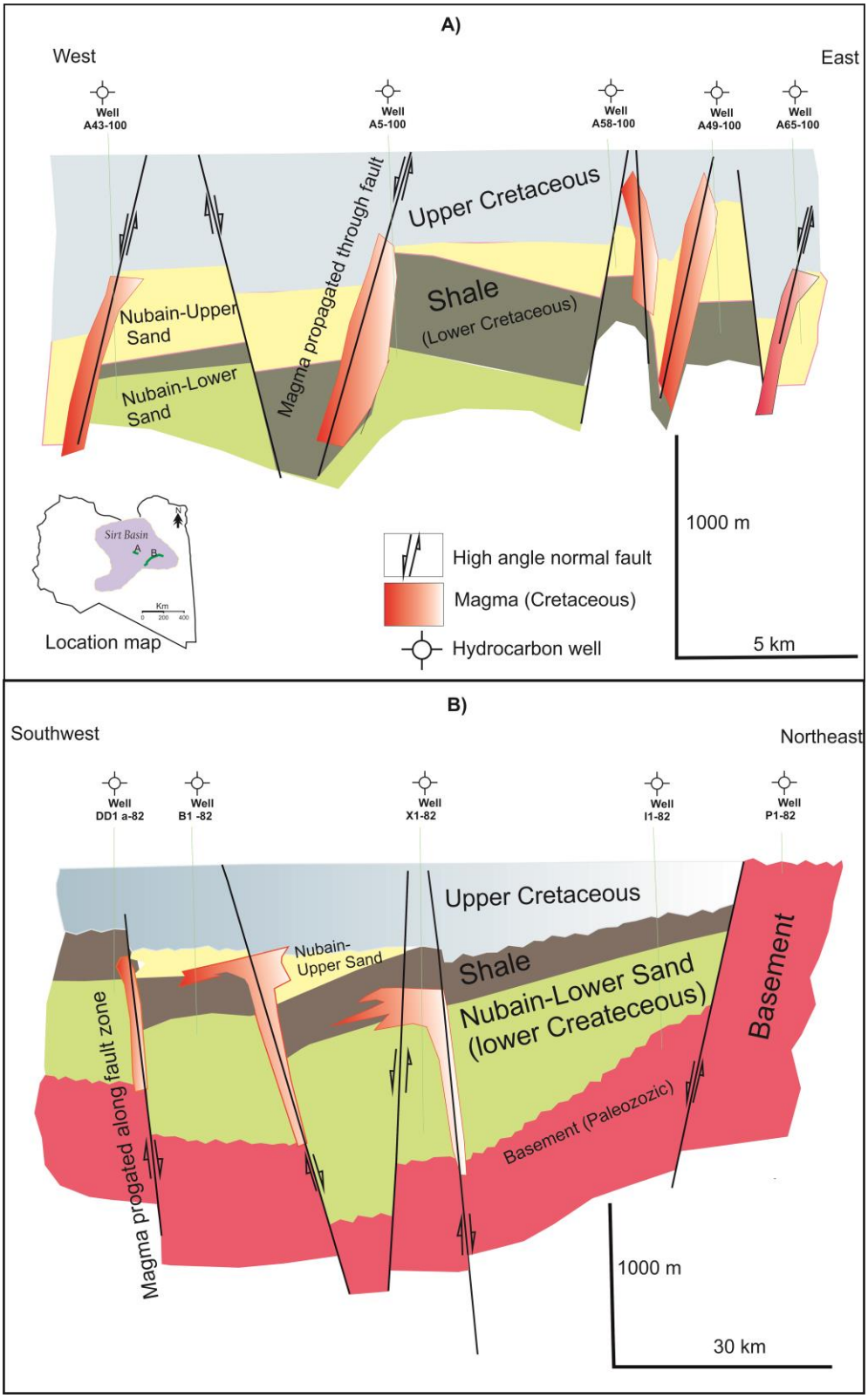

Fig. 13 *Cross sections inferred from boreholes data in the Al Hameimat Trough, SE Sirt Basin. Both cross sections, a and b, show high-angle normal faults, some of which may have acted as channels for magma, that is, parts of dyke paths (modified after Busrewil et al., 2012).*

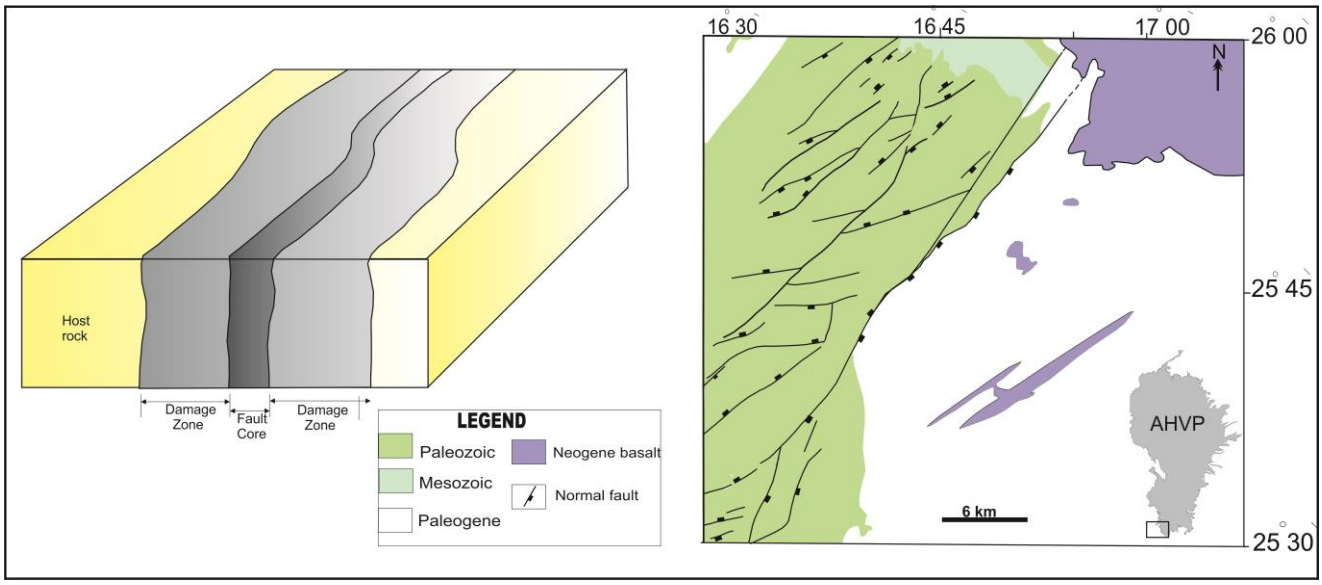

Fig. 14 *Left: schematic model of the internal structure of a fault zone (here a strike-slip fault) consisting of a damage zone and a fault core (modified after Gudmundsson et al., 2010). Right: geological map showing part of pre-existing normal faults (Palaeozoic and Mesozoic) that may have very stiff cores favouring dykes using the faults as parts of their paths (modified from Less et al., 2006).*

When a dyke approaches a mechanically weak discontinuity (i.e., one with low tensile strength) such as an active fault, the dyke may open up the discontinuity and, depending on the magmatic overpressure and the local stress field, enter the discontinuity. This is known from field observations and also from numerical models. For example, many dykes have been observed to follow steep normal faults for a while, both in the active and in the palaeo-rift zones of Iceland (Gudmundsson, 1995). Numerical models (Gudmundsson et al., 2010) show that a dyke meeting with a steep and mechanically weak normal fault tends to open up the fault and then use it as a part of the dyke path. Thus, although most dykes do not use faults as channels, the potential for a steep, active and weak normal fault to form a part of a dyke path is well established.

To explore this possibility further, we considered the interaction between a mechanically strong fault and a propagating dyke. More specifically, we model the core of the fault as stiff in relation to the damage zone. The idea here is to test if such fault zones might also function as a channel for magma. The core may become stiff primarily in two ways. First, through compaction and secondary mineralisation; second, through being injected by earlier dykes. It is the latter that we focus on here, given that many dykes are multiple and formed over considerable periods of time (Gudmundsson, 1995).

In the model, the fault zone is thus divided into a comparatively stiff core and soft damage subzones on either side of the core (cf. Browning and Gudmundsson, 2015; Fig.15). The only loading is magmatic overpressure of 10MPa in the dyke, as estimated above. The rock hosting the fault zone has a Young's modulus of 20GPa, and Poisson's ratio 0.25, both of which are typical values for rocks similar to those in the Sirt Basin. In the first model (Fig. 15a) Young's modulus of the core is 10GPa, and that of the damage subzones 1GPa, whereas in the second model (Fig. 15c), the core is made very stiff (30GPa). The models thus assume strain hardening, that is, a core that is stiffer (perhaps due do mineralisation and/or compaction or earlier dykes) than the damage zone. The numerical results (Fig.15b, d) indicate that for both models the trajectories of maximum principal stress field σ_1 tend to rotate and become deflected towards the fault plane, suggesting that the fault may capture the dyke propagation path for a while. These numerical results imply that local stress field may, from time to time, favour dyke propagation along the fault zone, both for soft as well as for stiff steep normal faults, in which case the faults may have acted as parts of the dyke paths to the surface.

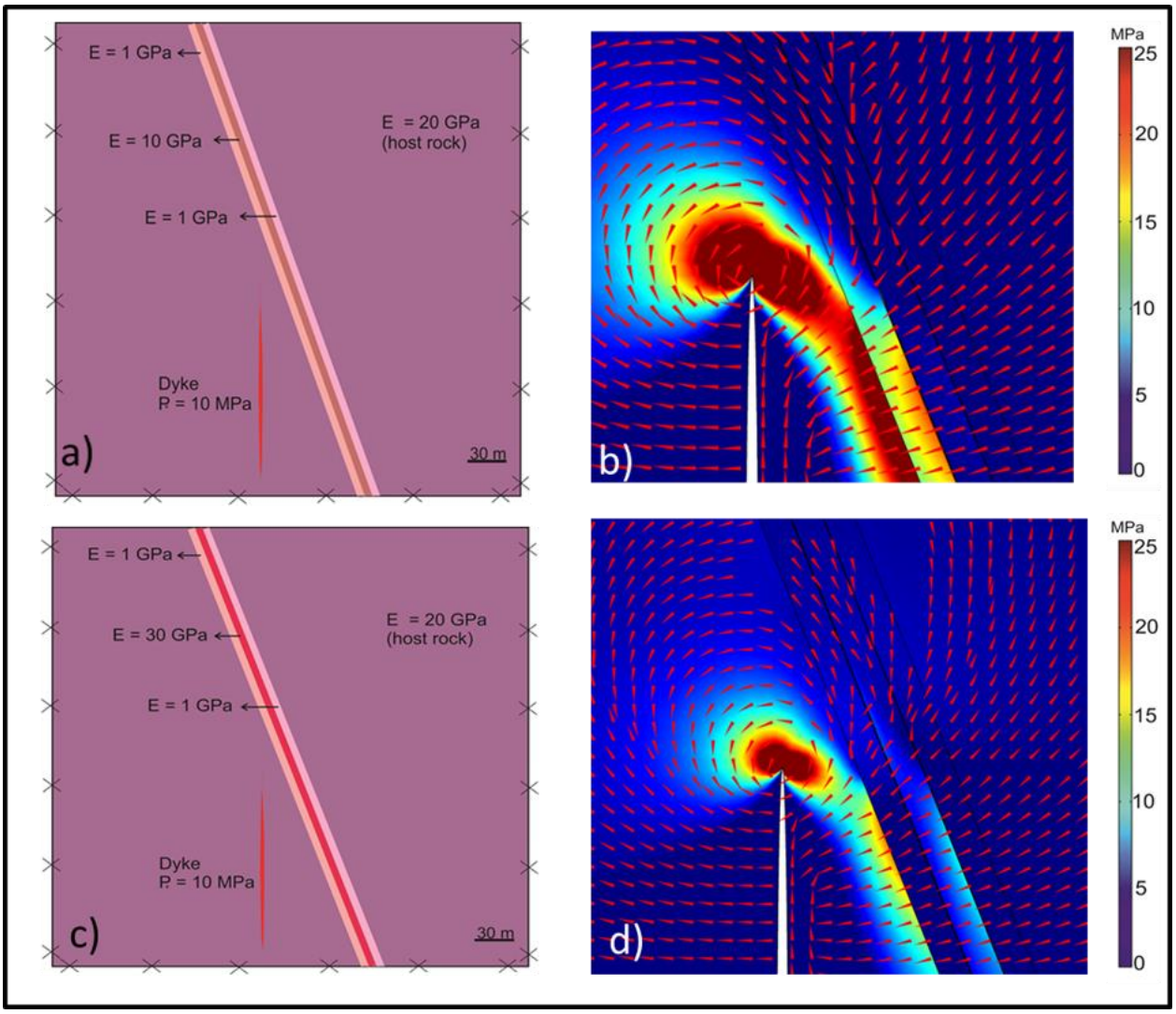

Fig. 15 *a) Setup showing how the host rock and fault zone are modelled using different values for Young's modulus. The fault zone is modelled as a high-angle normal fault, similar in attitude to many normal faults observed in Al Haruj region and the Sirt Basin. b) Results of the numerical models. Large tensile stress* σ_3 *occurs in the area between dyke tip and fault plane. Trajectories of maximum principal stress* σ_1 *are rotated and could deflect the magma/dyke path into the fault plane. This and subsequent numerical model reveal the variation in the local stresses within fault zones. c) The fault core is modelled as a stiff layer (red layer) to simulate strain hardening (mineralisation, compaction) and/or previous dyke intrusions. d) Numerical model results displaying maximum compressive principal stress* σ_1 *are clearly deflected towards the fault plane.*

9.2 Future volcano-tectonic activity of the AHVP

Many of the volcanic features of the AHVP, particularly in its northern subzone, appear very recent, based on well-preserved inflation features such as tumuli and lava rises as well as modern age dating by Nixon et al., (2014) who concluded that the youngest lava flows are of late Holocene age (2.31 ka). It follows that it is likely that the AHVP has still the potential to erupt, that is, is still active. One indication of volcano-tectonic activity is earthquakes. An earthquake network, however, was established only very recently (past decade) in Libya, and given that there is generally not much seismic activity in the country, the information is so far limited.

Data on historical earthquakes have, however, been collected. And some of the recorded earthquakes may be associated with magmatism. For example, earthquake swarms have been reordered in Hun Graben (northwestern Libya, Fig. 2) with earthquake magnitudes >M7.1 in 1935 and >M6 in 1939, 1940, 2000 and 2001, respectively (Hassen, 1983; Al-Heety, 2011). Earthquake swarms in volcanic regions are commonly related to magma migration, and could be so in these cases as well. Since the Hun Graben extends to the AHVP, the earthquake swarms, at least some of them, may be related to active magma migration beneath or close to the AHVP. Also, earthquakes on active faults are commonly triggered by high fluid pressure. If some of the faults are used as paths for magma in AHVP (Bagnardi, 2014), the magmatic pressure along the faults would tend to trigger slip on the faults and earthquakes. All these will become better established in the coming years as the new seismic network in Libya collects more earthquake data. While it is not certain, it seems

plausible that the AHVP is still being volcanically and tectonically active (Bardintzeff et al., 2012; Boote 2012).

10 Conclusions

- The Al Haruj Intra-continental Volcanic Province (AHVP) in Libya is the largest part of an extensive volcanic province, covering an area of approximately 42,000km^2. It is likely that the AHVP developed primarily during the early Pliocene to late Pleistocene, in response to tectonic rifting and evolution of the Sirt Basin, but it may still be active. Considerable attention has been focused on the AHVP in the last three decades, particularly with respect to its stratigraphy, geochemistry and geochronology. By contrast, volcano-tectonics of the area has received very little attention.

- The spatial distribution of around 432 eruption points or centres in the AHVP shows clustered distributions. Alignments of points/centres suggest that pre-existing structures, mainly along WNW to NW late Mesozoic-Cenozoic structures and along NE to NNE late Palaeozoic- early Mesozoic structures, exert some influence on the preferential of a magma pathway to reach the surface. The spatial distributions of volcanic eruptions reveal the presence of two maxima clustering of volcanoes.

- Volcanic fissures/crater rows are very common in the AHVP and mostly confined to the central and southernmost part of this region. Comparatively few dykes have been identified, but those that have occur mainly in elongated swarms outside the main volcanic system. The geometry of the volcanoes may be partly governed by pre-

existing fractures and faults; which in turn play a significant role in the spatial distribution of volcanic fissures and dykes in the area.

- The magmatic overpressure of 47 dykes and volcanic fissures is estimated based on their aspect (trace length/thickness) ratios. Most of the obtained values indicate overpressures between around 8MPa (when host-rock Young's modulus E = 7GPa) and 19MPa (when host-rock Young's modulus E = 15GPa). These results are very reasonable and similar to those obtained from basaltic dykes in other volcanic regions

- Numerical models were made to explore the local stress field around and within a fault zone when a dyke approaches it. In the models, the fault zone is divided into a comparatively stiff core (attributed to strain hardening) and softer damage zones on either side of the core. The numerical results indicate that the trajectories of maximum principal stress field σ_1 tend to rotate and become deflected towards the fault plane. Our findings suggest that steeply dipping faults, particularly normal faults, may capture propagating dykes for a while and act as parts of their paths.

Acknowledgements

AE thanks the Libyan Ministry of Higher Education for the financial support and John Browning and Marco Neri for very helpful review comments.

References

Abadi, A.M., van Wees, J.D., van Dijk, P.M., Cloetingh, S.A.P.L., 2008. Tectonics and subsidence evolution of the Sirt Basin, Libya. Am. Ass. Petrol. Geol. Bulletin 92, 993-1027.

Abdunaser, K., McCaffrey, K., 2014. Rift architecture and evolution: the Sirt Basin, Libya: the influence of basement fabrics and oblique tectonics. J. Afr. Earth Sci. 100, 203-226.

Abdunaser, K, McCaffrey, K., 2015. Tectonic history and structural development of the Zallah-Dur al Abd Sub-basin, western Sirt Basin, Libya. J. Struct. Geol. 73 (2015) 33-48.

Abebe, T., Mazzarini, F., Innocenti, F., Manetti, P., 1998. The Yerer Tullu Wellel volcano-tectonic lineament: a transtensional structure in central Ethiopia and the associated magmatic activity. J. Afr. Earth Sci. 26, 135-150.

Al-Hafdh, N. El-Shaafi, A., 2015. Geochemistry and petrology of basic volcanic rocks of Jabal Al Haruj al-Aswad, Libya. Int. J. Geosci. 6, 109-144. doi: 10.4236/ijg.2015.61008.

Al-Heety E., 2011. Seismicity and seismotectonics of Libya: as an example of intraplate environment. Arab J Geosci. (2011) 6:193–204 DOI 10.1007/s12517-011-0347-y.

Ambrose, G., 2000. The geology and hydrocarbon habitat of the Sarir Sandstone, SE Sirt Basin, Libya. J. Pet. Geol. 23, 165-191.

Anketell, M., 1996. Structural history of the Sirt Basin and its relationship to the Sabratah Basin and Cyrenaican Platform, northern Libya, in M., Salem, M.,. Busrewil, A., Misallati, A., and Sola, M., (Eds)., The Geology of Libya.

Babiker, M., Gudmundsson, A., 2004. Geometry, structure and emplacement of mafic dykes in the Red Sea Hills, Sudan. J. Afr. Earth Sci. 38,279–292.

Bagnardi, M., 2014. Dynamics of Magma Supply, Storage and Migration at Basaltic Volcanoes: Geophysical Studies of the Galápagos and Hawaiian Volcanoes. PhD thesis. University of Miami, USE. Scholarly Repository. Electronic Theses and Dissertations.

Bardintzeff, J., Deniel, H. Guillou, B. Platevoet, P., Oun, K., 2012. Miocene to recent alkaline volcanism between Al Haruj and Waw an Namous (southern Libya) Int. J. Earth Sci., 101 (2012), pp. 1047–1063.

Barnett, Z., Gudmundsson, A. 2014. Numerical modelling of dykes deflected into sills to form a magma chamber. J. Volcanol. Geotherm. Res. 281 (2014) 1–11.

Becerril, L., Galindo L., Gudmundsson, A. Marales J., 2013. Depth of origin of magma in eruptions. Scientific reports. 3 : 2762 | DOI: 10.1038/srep02762.

Bedard, J., Naslund H., Nabelek P., Winpenny A., Hryciuk M., Macdonald W., Hayes B., Steigerwaldt K., Hadlari T., Rainbird R., Dewing K., Girard E., 2012. Fault-mediated melt ascent in a Neoproterozoic continental flood basalt province, the Franklin sills, Victoria Island, Canada. Geol. Soc. Am. Bull. 124:723–736.

Boote, D., Dardour, A., Green, P., Smewing, J., Van Hoeflaken, F., 2012. Burial and unroofing history of the base Tanezzuft 'hot' Shale source rock, Murzuq Basin, SW Libya: new AFTA constraints from basin margin outcrops. In: 4th Sedimentary Basins of Libya Symposium: The Geology of Southern Libya, 17–20th November 2008, Tripoli, Libya.

Browning, J., Gudmundsson, A., 2015. Caldera faults capture and deflect inclined sheets: an alternative mechanism of ring dike formation. Bull Volcano (2015) 77: 4DOI 10.1007/s00445-014-0889-4.

Browning, J., Drymoni, K., Gudmundsson, A., 2015. Forecasting magma-chamber rupture at Santorini volcano, Greece. Scientific Reports. . doi: 10.1038/srep15785.

Burke, K., 1996. The African plate, South African J. Geol., 99, 341 – 409.

Busrewil, M., Suwesi, K., 1993. Geological Map of Libya 1: 250.000, Sheet : Al Haruj Al Aswad NG(33-4). Explanatory Booklet. Industrial Research Centre, Tripoli, p. 95.

Busrewil, M., 1996. The volcanology of central Jabal al Haruj al Aswad volcanic province, Central Libya. The geology of Sirt Basin, Elsevier, Amsterdam. Vol. III, P. 331-345 pp.

Busrewil , M., 2012. Evolution of Al Haruj Volcanic Province, Central Libya. Geology of Southern Libya, 2012, vol. 3.

Busrewil, M., Oun, K. Haman, M., 2012. Petrology and Tectonic Setting of Hameimaat Magmatic Rocks, SE Sirt Basin, Libya. Geology of Southern Libya, 2012, vol. 3, pp 189-210.

Cartwright, J., Hansen, M., 2006. Magma transport through the crust via interconnected sill complexes. Geology 34, 929–932.

Chen N., Dong J. Chen J., Dong C., Shen Z., 2014. Geometry and emplacement of the Late Cretaceous mafic dyke swarms on the islands in Zhejiang Province, Southeast China: Insights from high-resolution satellite images, J. Asian Earth Sci. 7 (2014) 302–311.

Cvetkovic´ , V., Toljic´ , M., Ammar, A., Rundic´ , L., Trish, K.B., 2010. Petrogenesis of the eastern part of the Al Haruj basalts (Libya). J. Afric. Sci. 58, 37–50.

Delaney, P., Pollard D., 1981. Deformation of host rocks and flow of magma during growth of minette dikes and breccia-bearing intrusions near Ship Rock, New Mexico, U.S. Geol. Surv. Prof. Pap. 1202.

Delaney P., Pollard D., ZIony I., McKee H., 1986. Field relations between dikes and joints: emplacement processes and paleostress analysis. J Geophys. Res. 91:4920–4938.

Drury, S., 2001. Image Interpretation in Geology. Blackwell Science, Nelson Thornes,UK, p. 290.

Farahat, S., Abdel Ghani, S., Aboazom, S., Asran, H., 2006. Mineral chemistry of Al Haruj low-volcanicity rift basalts, Libya: implications for petrogenetic and geotectonic evolution. J. Afric. Sci. 45, 198–212.

Francesco, M., D'Orazio, M., 2003. Spatial distribution of cones and satellite-detected lineaments in the Pali Aike Volcanic Field (southernmost Patagonia):insights into the tectonic setting of a Neogene rift system. J. Volcanol. Geotherm. Res. 125, 291-305.

Geshi, N., Kusumoto, S., Gudmundsson, A., 2010. Geometric difference between nonfeeders and feeder dikes. Geology 38, 195–198.

Gudmundsson, A., 1990. Emplacement of dikes, sills, and crustal magma chambers at divergent plate boundaries. Tectonophysics 176, 257–275.

Gudmundsson, A., 1995. Infrastructure and mechanics of volcanic systems in Iceland. J. Volcanol. Geotherm. Res. 64, 1–22.

Gudmundsson, A., 2011a. Rock Fractures in Geological processes. Cambridge University Press, Cambridge. doi:10.1017/ CBO9780511975684.

Gudmundsson, A., 2011b. Deflection of dykes into sills at discontinuities and magma chamber formation. Tectonophysics 500, 50–64.

Gudmundsson, A., Løtveit, I., 2012. Sills as fractured hydrocarbon reservoirs: examples and models. Geol. Soc. Lond., Spec. Publ. 374. http://dx.doi.org/10.1144/SP374.5.

Gudmundsson, A., Simmenes, T., Larsen, B., Philipp, S., 2010. Effects of internal structure and local stresses on fracture propagation, deflection,and arrest in fault zones. J. Struct. Geol. 32, 1643–1655.

Gudmundsson, A., Lecoeur, N., Mohajeri, N., Thordarson, T., 2014. Dike emplacement at Bardarbunga, Iceland, induces unusual stress changes, caldera deformation, and earthquakes. Bull. Volcanol., 76, 869. doi 10.1007/s00445-0869-9.

Hansen, M., Cartwright, J., 2006. Saucer-shaped sill with lobatemorphology revealed by 3D seismic data: implications for resolving a shallow-level sill emplacement mechanism. J. Geol. Soc. Lond. 163, 509–523.

Hasen, H., 1983. Seismicity of Libya and related problems. Master thesis. Civil Engineer Department, Colorado state University. Pp 108.

He M.,, Hutchinson J., 1989. Crack deflection at an interface between dissimilar elastic materials. Int. J Solids Struct. 31:3443–3455.

Holt, S., Holford. S., Foden, J., 2014. New insights into the magmatic plumbing system of the South Australian Quaternary Basalt province from 3Dseismic and geochemical data Australian Journal of Earth Sciences, 60, 797–816, http://dx.doi.org/10.1080/08120099.2013.865143.

Hutchinson, J.W., 1996. Stresses and failure modes in thin films and multilayers. Notes for a Dcamm CourseTechincal University of Denmark, Lyng by, (1–45pp.).

Klitzsch, E., 2000. The structural development of the Murzuq and Kufra basins - significance for oil and mineral exploration. Symposium on Geological Exploration in Murzuq Basin (Eds. M.A. Sola and D. Worsley), Elsevier, Amsterdam, p. 143-150.

Kusumoto, S., Geshi, N., Gudmundsson, A., 2013. Aspect ratios and magma overpressures of non-feeder dikes observed in the Miyake-jima volcano (Japan), and fracture toughness of its upper part. Geophys. Res. Lett. 40 (1–5), http://dx.doi.org/10.1002/grl.50284.

Le Corvec, N., Sporl., B. Rowland, J., Lindsay, J., 2013. Spatial distribution and alignments of volcanic centers: clues to the formation of monogenetic volcanic fields. Earth-Sci. Rev. 124, 96–114.

Less, Gy., Turki, S. M., Suwesi, S. Kh., Peregi, L. F., Koloszar, L., Kalmar, J., Sherif, Kh., Csaszar, G., Gulasci, Z., Dalum, H., Al Tajuri, A., 2006. Explanatory Booklet. Geological Map of Libya 1 : 250.000. Sheet : Waw Al Kabir NG 33- 12. Industrial Research Centre, 295 p.

Lesti, C., Giordano, G., Salvini, F., Cas R., 2008. Volcano tectonic setting of the intraplate, Pliocene-Holocene, Newer Volcanic Province (southeast Australia): Role of crustal fracture zones. Journal of Geophysical Research, Vol. 113, B07407, doi:10.1029/2007JB005110, 2008.

Nixon, S., Maclennan, J., White, N., 2014. Intra-plate magmatism of the Al Haruj Volcanic Field, Libya. Goldschmidt Conference Abstracts.

Magee, C, Jackson, C., Schofield, N., 2013. The influence of normal fault geometry on igneous sill emplacement and morphology. Geology 41:407–410.

Martin U., Ne´meth K., 2006. How Strombolian is a ‘‘Strombolian’’ scoria cone? Some irregularities in scoria cone architecture from the Transmexican Volcanic Belt, near Volca´n Ceboruco, (Mexico) and Al Haruj (Libya). J Volcanol. Geotherm. Res. 155(1–2):104–118.

Mohamed, M., 2014. Composition and Age of Cenozoic Volcanism in Libya. PhD thesis. University of Glasgow. Glasgow Theses Service.

Mouzughi, J., Taleb, T., 1981. Tectonic Elements of Libya (1:2,000,000). National Oil Corporation of Libya.

Pacific Aero Survey Co., 1979. Air bone Geophysical Survey Jabal Al Haruj Al Aswad Area. Final Report. Qeb., Inc. Hayward , California, 29 p.

Paulsen, T., Wilson, T., 2009. Structure and age of volcanic fissures on Mount Morning: a new constraint on Neogene to contemporary stress in the West Antarctic Rift, southern Victoria Land, Antarctica. Geological Society of America. 1071-1089.

Peregi, Zs., Less, G. Y., Konrad, Gy., Fodor, L., Gulacsi, Z., Gyalog, L., Turki, S. M., Suwesi, S. Kh., Sherif, Kh., Dalub, H., 2003. Explanatory Booklet. Geological Map of Libya 1: 250.000. Sheet: Al Haruj Al Abyad NG 33-8. Industrial Research Centre, Tripoli, 248 p.

Planke, S., Rasmussen, T., Rey, S., Myklebust, R., 2005. Seismic characteristics and distribution of volcanic intrusions and hydrothermal vent complexes in the Vøring and Møre Basins. In: Doré, A.G., Vining, B.A. (Eds.).

Poland, P., Moats, P., Fink H., 2008. A model for radial dike emplacement in composite cones based on observations from Summer Coon volcano, Colorado, USA, Bull. Volcanol., 70, 861–875, doi:10.1007/s00445-007-0175-9.

Polteau, S., Ferré, C., Planke, S., Neumann, R., Chevallier, L., 2008. How are saucer shaped sills emplaced? Constraints from the Golden Valley Sill, South Africa. J. Geophys. Res. 113, B12104. http://dx.doi.org/10.1029/2008JB005620 (Article number B12104).

Qui, K., Gherryo, Y., Shatwan, M., Fuller, J., 2008. The application of the Mechanical Earth Model on Rejuvenation of A Mature Field in Libya. Copyright 2008, IADC/SPE Asia Pacific Drilling Technology Conference and Exhibition, Jakarta, Indonesia, 16 p.

Rajesh, M., 2004. Application of remote sensing and GIS in mineral resource mapping an overview. J. Mineral. Petrol. Sci. 99, 83–103.Tabatabaian, M., 2014. Comsol for Engineers. Mercury Learning and Information, Boston.

Thomson, K., Schofield, N., 2008. Lithological and structural controlson the emplacement and morphology of sills in sedimentary basins. Journal of the Geological Society, London, Special Publications 302, 31–44.

Thouless, M., Parmigiani, J., 2007. Mixed-mode cohesive-zone models for delamination and deflection in composites. In: B. F. Sørensen, L. P. Mikkelson, H. Lilhot, S. Goutianos, and F. S. Abdul-Mahdi (Editors), Proceedings of the 28th Risø International Symposium on Materials Science: Interface Design of Polymer Matrix Composites. Roskilde (Denmark), pp. 93-111.

Tibaldi, A., 2015. Structure of volcano plumbing systems: A review of multi-parametric effects. Journal of Vol. Geotherm, Res. 298 (2015) 85–135. http://dx.doi.org/10.1016/j.jvolgeores.2015.03.023.

Wise, U., Funicello, R., Parotto, M., Salvini, F., 1985. Topographic lineament swarms: clues to their origin from domain analysis of Italy. Geol. Soc. Am. Bull. 96, 952-967.

Zakir, A., Quari, T., Mostafa, E., 1999. New optimizing technique for preparing lineament density maps. Int. J. Remote Sens. 20, 1073-1085.